Interface-limited injection in amorphous organic semiconductors

M. A. Baldo and S. R. Forrest
Center for Photonics and Optoelectronic Materials (POEM), Department of Electrical Engineering and the Princeton Materials Institute, Princeton University, Princeton, New Jersey 08544

(Received 30 June 2000; revised manuscript received 14 December 2000; published 7 August 2001)

We examine electron transport in the archetype amorphous organic material tris(8-hydroxyquinoline) aluminum (Alq_3). It is established that for Al, LiF/Al, and Mg:Ag cathodes, injection processes at the metal/organic contact dominate the current-voltage characteristics. We find that transport is also injection-limited at low temperatures, but that the cathode dependence of current-voltage characteristics at $T=30$ K is substantially reduced, raising doubts over metal-to-organic injection models that depend on the cathode work function. Given that ultraviolet photoelectron spectroscopy measurements show a shift in the vacuum potential at the metal/Alq_3 interface of ~ 1 eV, we investigate the impact of interfacial dipoles on adjacent molecules in the organic film. Consequently, we propose that injection is limited by charge hopping out of interfacial molecular sites whose energy distribution is broadened by local disorder in the interfacial dipole field. We derive a general analytic model of injection from interfacial states and find that it accurately predicts the current-voltage characteristics of transport in Alq_3 over many orders of magnitude in current and over a wide range of temperatures. The model is extended to other amorphous organic semiconductors and is found to be applicable to both polymers and small molecular weight organic compounds.

DOI: 10.1103/PhysRevB.64.085201 PACS number(s): 73.50.Gr, 73.40.−c, 73.61.Ph

I. INTRODUCTION

Charge transport in amorphous organic semiconductors is characterized by the localization of electronic states to individual molecules, and disorder in the position and the energy levels of those molecules. As a result, charge transport occurs via thermally activated hops with a mobility that typically increases with both electric field and temperature. Because of its widespread application to organic devices, tris(8-hydroxyquinoline) aluminum (Alq_3) has become an archetype material for studies[1–6] of electron transport in amorphous organic semiconductor thin films. Much progress has been made in analyzing bulk transport behavior in amorphous organic semiconductors such as Alq_3, and bulk transport characteristics are now well described for temperatures, $T \gtrsim 100$ K using a field and temperature-dependent mobility.[7,8]

Nevertheless, we demonstrate in this work that transport is injection-limited in thin Alq_3 films and devices. Thus, we cannot apply bulk-limited models such as trapped charge-limited transport[4,9–11] or space-charge-limited transport with a field and temperature-dependent mobility.[8] For example, bulk-limited models predict a dependence of current density J on thickness d, following $J \propto 1/d^x$ $(x \geqslant 1)$ at a constant electric field; however, no such dependence is observed here. Furthermore, although the temperature dependence of the current-voltage characteristics has been well fit to theories such as trapped-charge-limited models,[4,9–11] the agreement fails at low temperatures ($T < 100$ K). Finally, bulk-limited transport models cannot explain the dependence of current-voltage characteristics on the composition of the injection contact.

Nor does there appear to be a comprehensive model that fully explains current injection from contacts in a disordered organic semiconductor. As in the case of bulk models, an injection model should explain both the thickness and temperature dependencies of current-voltage characteristics over many orders of magnitude, and it should also explain the variations in injection for different cathode materials.[12] The absence of a model for charge injection into thin films of Alq_3 implies that important gaps remain in our understanding of the properties of this entire class of amorphous organic semiconducting materials.

Typically, transport over an interfacial barrier at a metal/semiconductor interface is analyzed using one of two theories. For very large barriers or at low temperatures, electron tunneling[13] has been thought to dominate the process. Alternately, if injection is thermally activated at room temperature, thermionic emission over the barrier is used to describe transport characteristics,[14] i.e.,

$$J = A^* T^2 \exp[-(\phi_B - \sqrt{qF/4\pi\varepsilon})/k_B T], \qquad (1)$$

where A^* is the modified Richardson constant, ϕ_B is the injection barrier, q is the electronic charge, F is the electric field, ε is the organic permittivity, k_B is Boltzmann's constant, and T is the temperature. But from fits to the injection characteristics of Alq_3 films, it was found that the prefactor A^* is approximately 10 orders of magnitude lower than the value calculated for a free electron.[1,13,15] Furthermore, although injection into Alq_3 is strongly thermally activated at room temperature (ruling out tunneling injection in this regime[4]), as we show below, the temperature dependence deviates from Arrhenius behavior for $T < 300$ K, and undergoes a marked transition at low temperatures ($T \sim 100$ K), becoming approximately temperature independent.

In their Monte Carlo simulations of thermionic injection at metal/organic interfaces, Wolf *et al.*[1] understand these discrepancies as consequences of the hopping process from a metal into an amorphous organic film with considerable dispersion in its molecular energy levels. But in contrast to the injection characteristics of Alq_3 and similar materials where

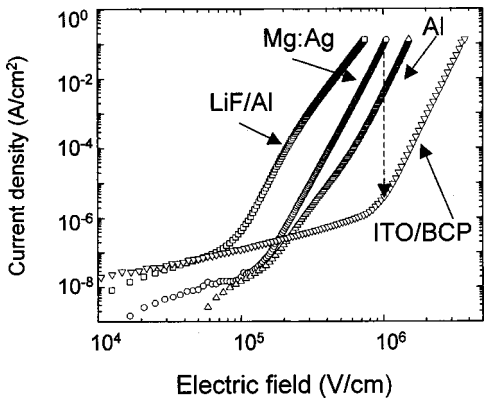

FIG. 1. Current density in Alq_3 as a function of applied electric field for a variety of different cathodes. The LiF/Al, Mg:Ag, and Al cathodes were fabricated as described in Sec. IV of the text; these devices had the general structure Mg:Ag anode/ 1200 Å Alq_3/cathode. The ITO/2,9-dimethyl-4,7 diphenyl-1,10-phenanthroline [bathocuproine (BCP)] device data is taken from Parthasarthy *et al.* (Ref. 17). The device structure was ITO anode/ 400 Å α-NPD/600 Å Alq_3/75 Å BCP/500 Å ITO. The ITO cathode was formed by depositing a thin (75 Å) layer of BCP on the Alq_3 and then depositing a further 500 Å of ITO by radio-frequency magnetron sputtering (Refs. 17 and 23). Despite the very large electron injection barrier in the ITO/BCP cathode, its injection efficiency at $F=10^6$ V/cm is only 10^5 less than the Mg:Ag device. The slopes of the Mg:Ag and ITO/BCP current-voltage characteristics are also similar.

transport is accurately described by a power law (i.e., $J \propto V^m$), the Monte Carlo simulations of Wolf *et al.*[1] do not generate these observed characteristics.

We also note that the efficiency of various injection cathodes does not follow the behavior expected if the initial hop from the metal Fermi level into the organic is the most energetically costly injection event.[1] For example, in Fig. 1, we show the current-voltage characteristics of Alq_3, with four commonly employed cathodes: LiF/Al, Mg:Ag, Al, and indium tin oxide (ITO). As previously observed elsewhere,[12,16,17] for increasing metal work functions, the injection efficiencies of the cathodes decrease (leaving aside the LiF/Al cathode for the moment, there is a consistent trend from Mg:Ag with a work function of $\phi_m=3.7$ eV;, to ITO with $\phi_m=4.7$ eV). But the slopes of the current-voltage characteristics are approximately independent of the work function, in contrast to the predictions of thermionic emission theory.[2] Moreover, the injection efficiency of these cathodes at a constant electric field should be exponentially dependent on the magnitude of the injection barrier; see Eq. (1). Given that the work function of ITO is 1 eV greater than that of Mg,[18] we would expect the injection efficiency (i.e., the current density at a given electric field) of the ITO cathode to be lower by a factor of $\sim 10^{18}$ at room temperature, when in fact it is observed to be lower by only $\sim 10^5$.

There are two possible explanations for these discrepancies: firstly, there may be intermediate states participating in the injection process, so that injection does not occur in a single hop; and secondly, interfacial dipoles at the contact may significantly alter the effective injection barrier for each cathode material. In this work, we show that these two explanations are related, and that *the presence of interfacial dipoles induces the intermediate states that participate in the injection process*. Supporting an organic interfacial injection model, we find that low temperature ($T\sim 30$K) transport is injection-limited but relatively independent of the cathode metal. While we cannot unambiguously discount the effects of extrinsic defects, we demonstrate that hopping out of a Gaussian distribution of intermediate states within the organic material near the metal injection interface yields current-voltage characteristics that closely approximate power-law behavior. But whereas previous power-law models were derived assuming bulk-limited transport requiring discrete conduction levels and traps, we are able to explain injection-limited power-law behavior for three commonly employed cathodes over the full range of working temperatures ($300\,\mathrm{K}>T>10\,\mathrm{K}$) using a hopping formalism and invoking only the intrinsic properties of the metal/organic interface.

In Sec. II we calculate the effect of dipoles at the metal/organic interface on the adjacent organic film. The net effect of the dipole layer is to lower the energies of the neighboring organic molecules relative to the bulk. We also find that disorder in the dipole layer leads to a significant broadening of the energetic distribution of neighboring organic sites, creating a reservoir of states for injected charges. We propose an analytic, microscopic model of hopping from these states in Sec. III. It is found that a Gaussian energy distribution of interfacial states with a half width of $\sigma\sim 0.4$ eV accounts for the current-voltage characteristics observed for a range of cathodes deposited on Alq_3. We demonstrate that this distribution is consistent with reasonable estimates of disorder in the orientation and magnitude of dipoles at the metal/organic interface. To further assess the merits of the proposed model, we compare its predictions to the characteristics of three cathodes commonly employed with Alq_3: LiF/Al, Mg:Ag, and Al. The fabrication of these devices is described in Sec. IV. From examination of the thickness dependence of charge transport, we confirm in Sec. V that at a thickness $d \lesssim 2000$ Å, conduction in Alq_3 is limited by interface injection mechanisms for all three cathodes. This result is verified by direct optical probing of the space-charge density using a thin phosphorescent-doped layer placed within the transporting medium. In Sec. VI we accurately fit the energetic distribution of the interface states to the Alq_3 current-voltage dependence on temperature from $T=10$ to 300 K using the interface-limited theory. This fit yields physically justifiable values for the Alq_3 intermolecular overlap and polaron binding energies. In Sec. VII we verify that the theory is self-consistent by applying these parameters to a Monte Carlo model of bulk transport, thereby obtaining calculated electron mobilities that compare well to time-of-flight measurements.[19] The theory is extended in Sec. VIII to injection at a metal/polymer interface, where we model the temperature dependence of hole injection into dialkoxy-PPV. Finally, we conclude in Sec. IX by discussing how the parameters characterizing hopping conductivity may be more accurately quantified.

TABLE I. Energies characteristic of several metal/Mq$_3$ interfaces.

UPS measurement[a]	Energy (eV)	Reference
Alq_3 ionization energy	(5.8 ± 0.1)	18, 26, 52
Alq_3 HOMO-LUMO gap	(4.6 ± 0.4)	54
Alq_3 optical gap	3.2	54
Mg work function	3.7	18
Al work function	4.0	18
Ag work function	4.3	18
ITO work function	4.7	18
Au work function	5.0	18
Interface dipole (Al/LiF/Alq_3)	1.7	18
	1.4	55
Interface dipole (Mg-Alq_3)	0.8	56
Interface dipole (Mg-Gaq_3)	(0.96 ± 0.1)	22
Interface dipole (Al-Alq_3)	1	18
Interface dipole (Ag-Alq_3)	1.1	18, 21
Interface dipole (Au-Alq_3)	1.1	18, 26, 52

[a]Summary data obtained by ultraviolet photoelectron spectroscopy (UPS) that are relevant to charge injection at metal/Mq$_3$ interfaces (M=Al, Ga). Most cathodes used in this work have the reverse orientation to those studied by UPS, that is, we deposit the metal on the organic film rather than depositing the organic on the metal; however, it is found for Mg and Al contacts that the injection characteristics of both metal/organic and organic/metal interfaces are identical if the surfaces are clean (Refs. 56 and 57). Measurements (Ref. 18) of an Al/5 Å LiF/Alq_3 interface find that the interfacial dipole between Al and the 5 Å LiF layer is 0.9 eV and that the interfacial dipole between the LiF and Alq_3 is 0.8 eV, giving a net interfacial dipole of 1.7 eV. Other measurements (Ref. 55) give a net dipole of 1.4 eV. Measurements at the Al/LiF interface are complicated by incomplete coverage of the 5-Å-thick LiF layer, and possible reactions between lithium ions and Alq_3 (Ref. 49). The Alq_3 HOMO-LUMO gap was distinguished from the Alq_3 optical gap by Hill *et al.* (Ref. 54) using UPS and inverse photoelectron spectroscopy and estimates of the electronic polarization energy for electrons and holes.

II. THE INTERFACE INJECTION MODEL

To identify the origin of the proposed interfacial states, we note that an abrupt and significant shift of approximately 1 eV in the vacuum level is observed at every metal cathode/Alq_3 interface studied to date using photoelectron spectroscopy[18,20,21] (see Table I). For example, the interfacial shift for Alq_3 on Al/LiF, Mg, Al, Ag, and Au is $\gtrsim$1 eV. Table I also lists the potential change at the interface between Mg and Gaq_3, the Ga analog of Alq_3 as it is expected to be similar to the Mg/Alq_3 interface.[22] The shift in the vacuum level is evidence for charge separation near the metal, forming dipoles at its interface with the underlying organic semiconductor. In addition, the organic material may possess extrinsic trap states due to impurities or damage introduced in the film deposition process[17,23,24] and cathode metal diffusion[25,26] into the organic. These extrinsic states influence charge transfer, perhaps explaining variations in the injection-limited current-voltage characteristics observed with different samples of Alq_3.[4,5] But irrespective of possible extrinsic effects, variations in the local dipole strength and orientation must result from randomness in the interface morphology, and the localization of charge in molecular materials. Disorder in the local interfacial dipole field significantly broadens the energy distribution of organic transport states in the interfacial layer, such that the initial hop from the metal Fermi level is *not* the most energetically costly injection event. Consequently, we can ignore the energy bar-

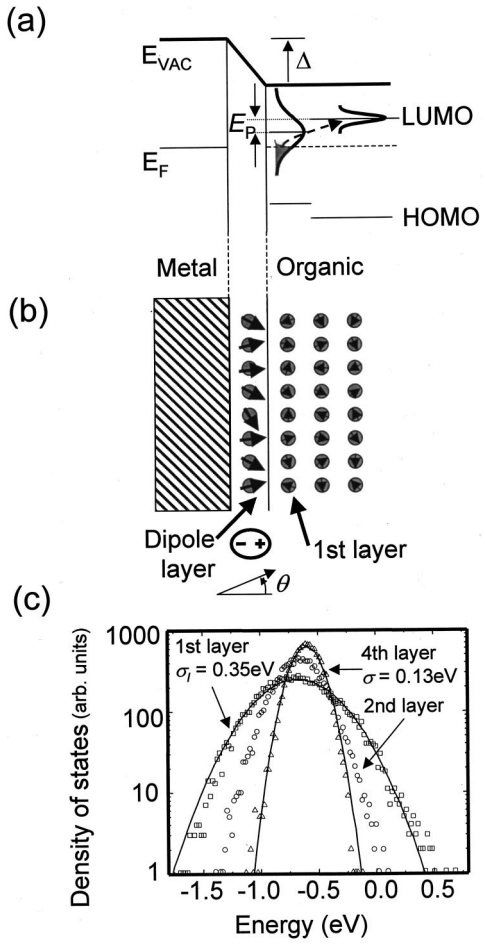

FIG. 2. (a) The injection model as a two-step process. Charges are initially injected into an interface region where the distribution of energy sites is broadened by interface dipoles, and lowered by E_P due to image charge effects. The limiting step is the hop from the interfacial region into the bulk distribution. (b) We model the interface in (a) by a collection of point dipoles. In the bulk, each site is randomly oriented with the Alq_3 dipole moment of $p=5.3$ D. But at the interface the dipoles are oriented in a Gaussian distribution about the perpendicular ($\theta=0$). It is likely that the strength of each dipole also varies, further randomizing the local dipole field. (c) The effect of the interface dipoles on the electron-energy distribution in the bulk is calculated. We find that the distribution in the first few organic monolayers is considerably broadened. For interface dipoles of $p=30$ D and a Gaussian angular distribution of width $\sigma_\theta=1.5$ rad, $\sigma_I=0.35$ eV. With increasing distance, the energetic distribution, approaches the bulk distribution $\sigma_B=0.13$ eV, with a mean energy of $E=0$ eV.

rier between the cathode and the interface states. We assume that charges from the metal are readily injected into a broad distribution of interfacial states from which they must hop into a narrower, higher energy distribution of transport states. This process is illustrated in Fig. 2(a), where we also show the expected energy levels in the presence of an interfacial dipole layer. Although transport is dominated in this case by the effects of disorder, electric field screening by the metal contact also reduces the lowest unoccupied molecular orbital (LUMO) and the highest occupied molecular orbital (HOMO) splitting energy at the interface by an amount $E_p \sim 0.2\,\mathrm{eV}$ relative to the bulk.[21] The variation in the mean energy of the transport states has been considered previously.[27]

It has been proposed that the energetic disorder in amorphous materials such as Alq_3 is due, in large part, to the randomly oriented dipole moments of the molecules.[28] For an infinite simple cubic lattice with lattice parameter a, the resulting site energy distribution is approximately Gaussian with a standard deviation related to the dipole moment p by[29]

$$\sigma_B = \frac{2.35qp}{4\pi\varepsilon a^2}. \tag{2}$$

For Alq_3 where $p = 5.3\,\mathrm{D}$, a standard deviation of $\sigma_B = 0.13\,\mathrm{eV}$ is thus obtained.[30]

Due to the anisotropy of the metal-organic interface we cannot use Eq. (2) to obtain the energy distribution adjacent to the cathode, and must instead numerically calculate[29] the density of states in this region. In Fig. 2(b) we represent the interfacial dipole layer as a collection of point dipoles. Hence, to estimate the effects of the dipole layer on the molecular density of states, we model the interface with an array of $101\times101\times15$ dipole sites with an intersite spacing of 10 Å, corresponding to a 150-Å-thick organic layer. To consider the effects of a variation in the angular distribution of the interfacial dipoles, we assumed that the dipoles possess a Gaussian angular distribution centered perpendicular to the contact ($\theta = 0$), and with an angular half width of σ_θ. We further assume that these dipoles have a strength of $p = 30\,\mathrm{D}$, corresponding to charges separated by ~6 Å, which is on the order of the expected metal-organic molecular separation at the contact interface. This dimension is also consistent with the dipole formed between an Alq_3 cation and its image in the cathode metal.

Given these parameters, the mean energy of the distribution is calculated to be −0.7 eV, consistent with the ~1 eV change in the vacuum level commonly observed at metal/Alq_3 interfaces (see Table I). With increasing distance from the interface, the center of the distribution approaches $E = 0$ eV (i.e., the bulk ''reference'' energy) and its width approaches the bulk distribution as calculated in Eq. (2) ($\sigma_B = 0.13\,\mathrm{eV}$). But as shown in Fig. 2(c), if the angular distribution of the interfacial dipoles is $\sigma_\theta = 1.5\,\mathrm{rad}$, we find that the energetic distribution of sites in the first organic layer is significantly broadened ($\sigma_I = 0.35\,\mathrm{eV}$) by the proximity of the dipoles. Alternately, a similar energetic distribution could be caused by variations in the strength of parallel dipoles.

On the molecular scale, the dipoles are not accurately represented as points; rather, we should examine charge separation across the interface and model individual charges on the molecules within the first organic layer. Nevertheless, the calculation of Fig. 2(c) is intended to demonstrate that dipoles at the metal/organic interface can significantly broaden and shift the energetic distribution of adjacent sites in the organic film from their bulk values. Indeed, we determine below that the injection properties of LiF/Al, Al, and Mg:Ag cathodes are well described by charge hopping out of such an energetically broadened interface layer with $\sigma_I \sim 0.4\,\mathrm{eV}$.

III. ANALYTIC HOPPING MODEL FOR CHARGE INJECTION FROM A GAUSSIAN DISTRIBUTION OF INTERFACE STATES

To fully describe the effects of the interfacial sites on charge injection, we note that the charge density per unit energy near the metal is determined by Fermi-Dirac statistics, viz.,

$$n_I(E_I,E_F) = \frac{N_I/\sqrt{2\pi\sigma_I^2}}{1+\exp[(E_I-E_F)/k_BT]}\exp\left[-\frac{1}{2}\left(\frac{E_I}{\sigma_I}\right)^2\right], \tag{3}$$

where N_I and E_I are the density and energy of interfacial sites, respectively, and E_F is the Fermi level. Assuming that hopping out of these sites limits the current density, the distribution of ''transport'' bulk sites can initially be considered to be empty.

Across the interface, the current density is given by

$$J(E_F) = \frac{\overline{a}q}{\sqrt{2\pi\sigma_B^2}}\int_{-\infty}^{\infty}\int_{-\infty}^{\infty} n_I(E_I,E_F)R(E_B-E_I-\overline{a}qF) \times\exp\left[-\frac{1}{2}\left(\frac{E_B}{\sigma_B}\right)^2\right]dE_I dE_B, \tag{4}$$

where the width of the bulk charge distribution is given by σ_B, E_B is the energy of the charge in the bulk, and $\overline{a}$ is the average intermolecular spacing. The hopping rate is $R(E)$, where E is the energy difference between adjacent hopping sites. The charge at the interface determines the electric field F, and voltage V, viz.,

$$V = \frac{qn_T d_I d}{\varepsilon}, \tag{5}$$

where n_T is obtained by integrating Eq. (3) over all E_I, and d_I is the thickness of the interfacial region containing filled sites. As expected for injection-limited transport, the bias voltage is linearly proportional to the thickness, at least for $d \gg d_I$.

To fully characterize the expected thickness dependence of the current-voltage characteristics of a thin organic film, we must also consider the alternative to injection-limited transport. As the thickness of the film increases, transport eventually becomes bulk limited, with

$$J = nq\mu F. \tag{6}$$

Because of the low density of free charge in these materials, the injected space charge determines the electric field under a bulk transport limit.[9] Assuming an approximately field-independent mobility μ, solving Eq. (6) together with Poisson's equation gives $V \propto d^{1.5}$ at constant J. If some charge is trapped, then the thickness dependence is $V \propto d^{x}$, where $1.5 \leqslant x \leqslant 2$. However, direct measurements of the mobility show that it is actually field dependent, and can be heuristically modeled (for $T > 100$ K) by Gill's expression[32]

$$\mu(F,T) = \mu_0 \exp(-E_0/k_B T_{\text{eff}}) \exp(\beta\sqrt{F}/k_B T_{\text{eff}}), \tag{7}$$

where $E_0 = k_B T_0$ is the activation energy for hopping at zero electric field, $1/T_{\text{eff}} = 1/T - 1/T_0$, and μ_0 and β are constants. Studies of charge transport in the conjugated polymer, poly(*p*-phenylenevinylene) (PPV) have observed space-charge limited transport with such a field dependent mobility.[8,32] Typically, the field dependence of mobility reduces x such that $1 < x < 1.5$ for bulk-limited transport.

Thus, by studying the thickness dependence of charge transport we can clearly discriminate between injection and bulk limits. For injection-limited transport, the voltage at a given current density should be proportional to the thickness, i.e., $V \propto d$. In addition, the thickness dependence of Eq. (6) should be examined at constant field F; for injection-limited transport, the current density J should be independent of thickness d. As above, for bulk-limited transport, we expect that $J \propto 1/d^{x}$, with $x \geqslant 1$.

The model is completed by describing the dependence of the hopping rate R on electric field and temperature. We assume the small polaron model of intermolecular hopping. Here the rate-limiting step is not the electron transfer between weakly interacting molecular orbitals, but rather the formation of an activated complex that precedes the transfer.[33–36] For a carrier to jump to an adjacent site, the local electronic energy level must momentarily coincide with that of a neighboring molecule.[37] Such a ''coincidence event'' generally requires a substantial instantaneous local distortion of the lattice.[37] Thus, polaron hopping requires consideration of phonon coupling to yield the correct activation energy. Here, we include interactions with an optical phonon mode of frequency ω_0 for zero wave vector. The rate is then given by[36]

$$R = \left(\frac{2\pi J_0^2}{\hbar^2 \omega_0}\right) e^{-2S} e^{-E/2k_B T} \sum_{n=-\infty}^{\infty} I_{|E|/\hbar\omega_0} \times \left\{ \left[\left(\frac{2E_b}{\hbar\omega_0} \right) A_n \operatorname{csch}(\hbar\omega_0/2k_B T) \right] - \delta_{E,0} \right\}, \tag{8}$$

where

$$S = (E_b/\hbar\omega_0)\cosh(\hbar\omega_0/2k_B T), \tag{9}$$

and $I_{|E|/\hbar\omega_0}$ is a modified Bessel function of order $|E|/\hbar\omega_0$; $2\pi\hbar$ is Planck's constant; J_0 is the electronic transfer integral related to the electron transport half bandwidth by $6J_0$;[36] and E_b is the small polaron binding energy in the limit of $J_0 = 0$ (i.e., no electronic overlap between adjacent molecules). The phonon bandwidth determines the relaxation amplitude coefficients A_n.[36] As a simplifying assumption, we take $A_n = \delta_{n,0}$, where $\delta_{n,0}$ is the Kronecker δ function which,[37] together with the use of Eq. (8) for continuous E,[38] implies a considerable dispersion in the phonon mode.

Polaron hopping exhibits two different regimes:[38] the low-temperature regime at $k_B T_P < \hbar\omega_0/3$, where[36,38]

$$R(E) \propto \exp\left(-\frac{E + |E|}{2k_B T} \right) \frac{(2E_b/\hbar\omega_0)^{|E|/\hbar\omega_0}}{(|E|/\hbar\omega_0)!}, \tag{10}$$

and at higher temperatures[38]

$$R(E) \propto (E_b k_B T)^{-1/2} \exp\left[-\frac{E_b}{2k_B T} \left(1 + \frac{E}{2E_b} \right)^2 \right]. \tag{11}$$

In the high temperature regime, hopping may be anazlyed classically; indeed the high temperature expression for polaron hopping [Eq. (11)] has the same form as the expression derived by Marcus[33] for electron transfer. The activation energy at high temperatures (the polaron binding energy), E_b, is related to the reorganization energy λ in the Marcus formalism by $E_b = \lambda/2$.[38] Marcus theory has been successfully applied to electron transfer reactions in chemistry and biology, and most of its key predictions have been experimentally confirmed,[39] notably the existence of an inverted region. As shown in Fig. 3(a), in the presence of low electric fields, the rate of electron transfer is limited by a barrier height of approximately $\lambda/4 = E_b/2$. At a somewhat higher field, resonant transfer is reached [see Fig. 3(b)]; but further increases in the field result in a decrease in rate—the ''inversion region'' [see Fig. 3(c)]. Marcus theory has also been used to describe the dependence of charge carrier mobility in solid amorphous organic materials on electric field and temperature.[38,40]

Note that Eq. (10) and Eq. (11) (where $0 < E \leqslant E_b$) may be approximated by ''Miller-Abrahams'' hopping, viz.:[38]

$$\begin{aligned} R(E) &= A_0 \exp(-E/k_B T), \quad E \geqslant 0 \\ R(E) &= A_0, \quad E \leqslant 0 \end{aligned} \tag{12}$$

where E is now the separation between sites, and A_0 is the maximum hopping rate determined by the intermolecular electronic orbital overlap. The simplification of Eq. (1) is frequently employed in studies of transport in amorphous solids, and is known as the Miller-Abrahams expression.[1] It consolidates the numerous parameters of the full polaron model into only one adjustable parameter, A_0, the maximum hopping rate. The approximation ignores the ''Marcus inversion'' region, which may occur in the classical region at high electric fields. However, since inversion is expected for $aqF > \lambda$, typical values of the intermolecular spacing, $a \sim 10$ Å, and reorganization energy, $\lambda \sim 0.2$ eV, give required electric fields for inversion of $F > 2 \times 10^6$ V/cm. Amorphous devices typically operate at $F < 2 \times 10^6$ V/cm, thus, the Miller-Abrahams model is probably well-suited to the analysis of charge transport in most organic devices. In this work we apply both the full polaron model and the Miller-Abrahams simplification to understand charge injection.

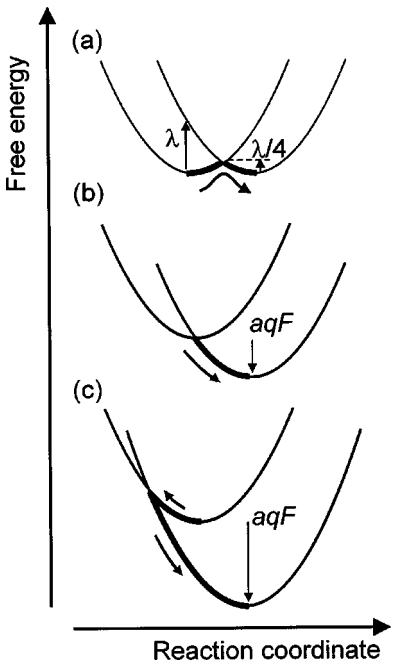

FIG. 3. (a) A representation in the high-temperature regime of polaron hopping between two identical molecules with the same ground-state energy. The process is identical to the Marcus electron transfer with a reorganization energy of $\lambda = 2E_b$, where the polaron binding energy is E_b. In the absence of changes in the atomic configurations, the barrier to electron transfer is $\lambda = 2E_b$; if, however, the molecules form an activated complex, then the energy barrier is reduced to $\lambda/4 = E_b/2$. (b) The electric field F increases the probability of charge transfer by reducing the energy barrier. As the field increases, the barrier is reduced until the transfer becomes resonant. (c) The transfer rate is inverted since $F > \lambda/aq$. Note that in an amorphous film, the ground-state energy levels of the molecules vary and the dispersion in energy may be on the order of E_b. This figure is adapted from Ref. 39.

In polaron formalism, the temperature dependence of hopping is affected by the temperature dependence of the phonon density. Below the phonon-induced transition temperature, $T_P \sim \hbar\omega_0/3k_B$, "downward" hops in Eq. (10) are temperature independent, whereas above T_P there is a strong temperature dependence in both upward and downward hops.[41] In fact, a transition in the temperature dependence is a general characteristic of transport in disordered materials, but alternative explanations have been advanced. Wolf *et al.*[1,6] note that if equilibrium is established, the mean energy of carriers in the organic solid lies at an energy σ^2/k_BT below the center of the Gaussian density of states. Thus, it was proposed that as temperature is decreased, the effective energy barrier to injection into a Gaussian density of states from a metal contact also decreases.

Whether or not equilibrium is established in the organic film (an issue addressed in Sec. VII), we note that disorder increases the variance of the density of states and hence the probability of temperature-independent hops. Thus, there are *two* processes that affect the temperature dependence of injection: energetic disorder, which determines the width of the density of states and the likelihood of resonant, temperature-independent hops, and the temperature dependence of the phonon distribution. For a charge carrier hopping from initial energy E_i to final energy E_f, the hopping model of Eqs. (11) and (4) gives

$$J \propto \int_{-\infty}^{\infty} \exp\left[-\frac{(2E_b + E_f - E_i)^2}{8E_b k_B T}\right] \exp\left[-\frac{1}{2}\left(\frac{E_f}{\sigma}\right)^2\right] dE_i$$

$$\propto \exp\left[-\frac{(2E_b - E_i)^2}{8E_b k_B T + 2\sigma^2}\right]. \tag{13}$$

From this expression we define a disorder-induced characteristic temperature

$$k_B T_D = \frac{\sigma^2}{4E_b}. \tag{14}$$

For $\sigma = 0.13\,\mathrm{eV}$ and typical values of the binding energy, $E_b \sim 0.2\,\mathrm{eV}$, the disorder-induced transition temperature is $T_D \sim 250\,\mathrm{K}$, significantly higher than the phonon-induced transition temperature. The disorder-induced transition temperature may also be calculated using the simplified Miller-Abrahams hopping model. For a charge carrier hopping from a discrete energy level into a distribution of sites, we define T_D as the temperature where the rate of downward hops equals that of upward hops. In this case

$$\int_{-\infty}^{-\Delta E} \exp\left[-\frac{1}{2}\left(\frac{E}{\sigma}\right)^2\right] dE$$

$$= \int_{-\Delta E}^{\infty} \exp\left(-\frac{\Delta E + E}{k_B T_D}\right) \exp\left[-\frac{1}{2}\left(\frac{E}{\sigma}\right)^2\right] dE. \tag{15}$$

Here the energy difference between the discrete energy level and the center of the distribution of sites is ΔE. If $\Delta E \gg \sigma \gg k_B T_D$ then it can be shown that Eq. (15) gives

$$k_B T_D = \frac{\sigma^2}{2\Delta E}. \tag{16}$$

As shown in Sec. VI, Eqs. (14) and (16) provide rough estimates of the temperature when the Arrhenius law governing charge transport breaks down.

IV. EXPERIMENTAL METHOD

In the following two sections we test the predictions of Sec. III by fabricating thin-film electron-injection-only amorphous Alq_3 devices. The device structure used in all measurements consists of an injecting cathode, a variable thickness layer of Alq_3, and a 1000-Å-thick 25:1 Mg:Ag anode to minimize hole injection. Materials were deposited by thermal evaporation under high vacuum ($<10^{-6}$ Torr). To prevent oxide formation on the anode, there was no vacuum break between its deposition and deposition of the Alq_3 layer. Cathodes consisted of either a 1000-Å-thick layer of Al, a 1000-Å-thick layer of 25:1 Mg:Ag with a further 300 Å of Ag for protection from oxidation,[16] or a 5 Å LiF layer followed by 1000 Å of Al.[12] Each cathode was defined by

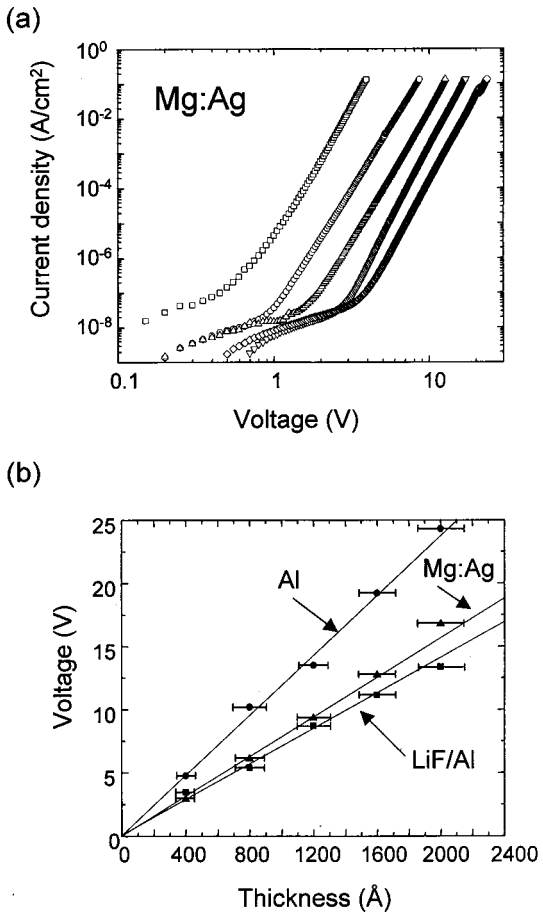

FIG. 4. (a) Thickness dependence of the current-voltage characteristics of Alq_3 films are shown for a Mg:Ag cathode. The device possessed a Mg:Ag anode beneath a layer of Alq_3. The total Alq_3 thickness was (□) 400 Å, (○) 800 Å, (△) 1200 Å, (▽) 1600 Å, and (◇) 2000 Å. The characteristics are parallel for approximately six orders of magnitude of current density, demonstrating a constant thickness dependence in this range. Similar characteristics are also observed for LiF/Al and Al cathodes. (b) Drive voltage (at a current density of $J=10\,\mathrm{mA/cm^2}$) as a function of Alq_3 thickness using LiF/Al, Mg:Ag, and Al cathodes. All three cathodes exhibit a linear thickness dependence for a thickness, $2000\,\text{Å} \gtrsim d \gtrsim 400\,\text{Å}$.

metal deposition through a shadow mask with 1-mm-diam holes. For room-temperature measurements, glass substrates were used; low-temperature measurements employed thermally conductive Si substrates with an additional 0.7-μm-thick surface layer of SiO_2 for electrical isolation.

Glass substrates were precleaned in a bath of deionized water and detergent and subjected to ultrasonic vibrations to remove dust and other microscopic particles, before being rinsed in sequential applications of deionized water, acetone, boiling trichloroethylene, acetone, and isopropanol. An aqueous solution of HF was used to etch away residual SiO_2 and to clean the silicon substrates. Optical measurements were performed in air, but in between measurements, completed devices were stored under a nitrogen atmosphere or in an evacuated cryostat to minimize oxidation of the cathode.

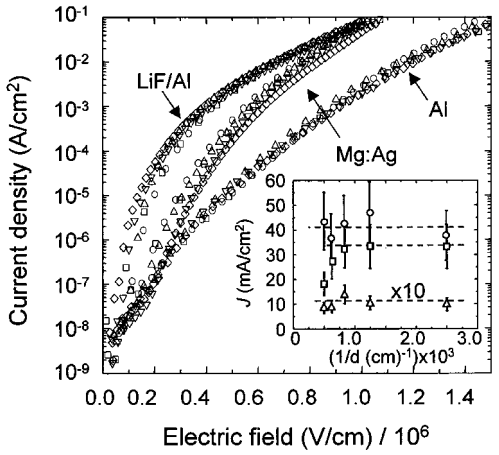

FIG. 5. The thickness data of Fig. 4 versus electric field, $F=V/d$. The differences between the various cathodes demonstrate the importance of the injection interface. The total Alq_3 thickness was (□) 400 Å, (○) 800 Å, (△) 1200 Å, (▽) 1600 Å, and (◇) 2000 Å. Inset: Current density at $F=9\times10^5$ V/cm versus the reciprocal of film thickness *d*. The current density is approximately constant as expected for injection-limited transport. The different cathodes are denoted by (□) LiF/Al, (○) Mg:Ag, and (△) Al, where the Al data have been multiplied by ten for clarity. Since a small change in voltage corresponds to a large change in the current density, small errors in the determination of the thickness lead to a substantial error in the determination of the current density at a constant field. The error corresponds to a 3% error in the film thickness.

V. DEPENDENCE OF TRANSPORT ON FILM THICKNESS AND SPACE-CHARGE DENSITY

The thickness dependence for Alq_3 with a Mg:Ag cathode is shown in Fig. 4(a). The current-voltage characteristics are parallel for Alq_3 films of varying thickness, demonstrating that the limiting transport process applies to current densities ranging over at least six orders of magnitude. Similar parallel slopes are observed in the characteristics of LiF/Al and Al cathodes. The data for each cathode are summarized in Fig. 4(b) by plotting the applied voltage at a current density of $J=0.01\,\mathrm{A/cm^2}$. The three cathodes show a linear dependence following $V \propto d$ consistent with Eq. (5) and injection-limited transport. The difference in the slopes of the thickness dependencies in Fig. 4(b) reflect the stored charge at each injection interface; assuming that the thickness of the interfacial region is the same in each case at $d_I=10\,\text{Å}$, we find that the interfacial density of charge is highest for the Al cathode ($n_I=2.0\times10^{19}\,\mathrm{cm^{-3}}$), and less for the Mg:Ag and LiF/Al cathodes (at $n_I=1.3\times10^{19}\,\mathrm{cm^{-3}}$ and $n_I=1.1\times10^{19}\,\mathrm{cm^{-3}}$, respectively).

To further confirm that the observed current-voltage characteristics are not bulk limited, in Fig. 5 we show the current density for each device in Fig. 4(b) plotted as a function of electric field, $F=V/d$. As expected for injection-limited transport, the three cathodes exhibit clearly different characteristics, and for a given cathode, transport is approximately independent of film thickness. This is demonstrated in the inset, where we plot current density for each cathode at a

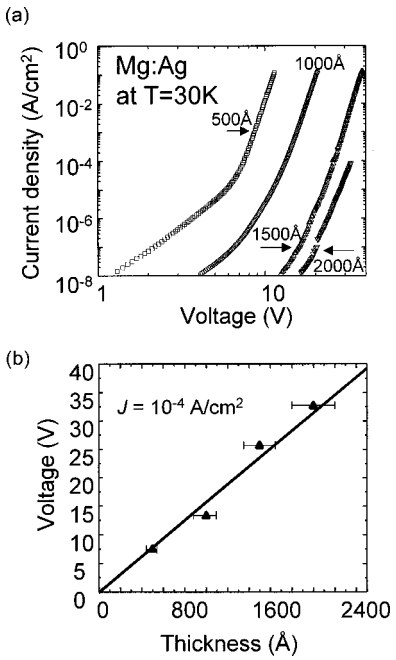

FIG. 6. (a) Thickness dependence of the current-voltage characteristics of Alq_3 films are shown for a Mg:Ag cathode at $T=30$ K. The device possessed a Mg:Ag anode beneath a layer of Alq_3. The total Alq_3 thicknenss was (□) 500 Å, (○) 1000 Å, (△) 1500 Å, and (▽) 2000 Å. The thickest device failed at $J=10^{-4}$ A/cm. **(b)** Drive voltage (at a current density of $J=10^{-4}$ A/cm^2) as a function of Alq_3 thickness at $T=30$ K. As with the room temperature characteristics, Mg:Ag cathodes exhibit a linear thickness dependence for a thickness, 2000 Å≥d≥500 Å.

field of 9×10^5 V/cm. For bulk-limited transport at constant field, we expect from Eq. (6) that $J\propto 1/d^x$, where $x\geqslant 1$, but for $d\lesssim 2000$ Å, this is not supported by the data. As the organic film thickness increases, transport must eventually become bulk limited, although this limitation is not relevant to most organic thin-film electronic devices[42] whose total thickness is typically ~1000 Å.

Figures 4 and 5 demonstrate that transport in Alq_3 is injection limited at room temperature for Al, Mg:Ag and LiF/Al cathodes. The thickness dependence of Alq_3 with a Mg:Ag cathode at $T=30$ K is shown in Fig. 6. Again, the current voltage characteristics shown in Fig. 6(a) are parallel, and in Fig. 6b, the V versus d data for a current density of $J=10^{-4}$ A/cm^2 are linear, indicating that transport is also injection-limited at low temperatures. However, we would expect at low temperatures that the electron mobility is a strong function of electric field [see Eq. (7)], giving a bulk-limited V vs d thickness dependence that may also approach a linear relationship. Given that transport is injection-limited at room temperature, the largest energy barrier to transport is at the injection interface; therefore, it is unlikely that the temperature dependence of the injection process is weaker than the temperature dependence of bulk transport.

Accordingly, we expect that transport in Alq_3 is injection limited for temperatures below room temperature. But even if transport is bulk-limited at low temperatures, the space charge will be confined at the injection interface by the strong dependence of mobility on electric field; thus, the interface-limited theory of Eq. (3), (4), and (5) holds for both injection and bulk-limited transport at low temperature.

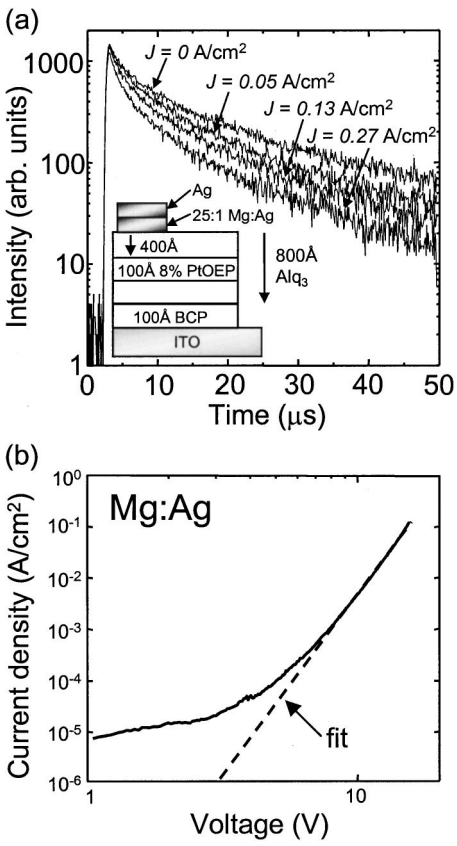

FIG. 7. (a) The transient phosphoresent decay of PtOEP at a wavelength of $\lambda=650$ nm in response to an optical pulse at $\lambda=532$ nm as a function of electron current. Under bias, no green electroluminescence from Alq_3 was observed, demonstrating monopolar electron transport. *Inset*: The device structure used to measure triplet-polaron quenching. (b) The J-V characteristics and structure of the device used to measure triplet-polaron quenching. To calculate the field dependence of mobility, the transport data were fit to $J=10^{-10}\times(F(0)d)^{7.6}$(A/cm^2) (dashed line).

The bulk space-charge density also varies according to whether transport in Alq_3 is injection or bulk limited. As a

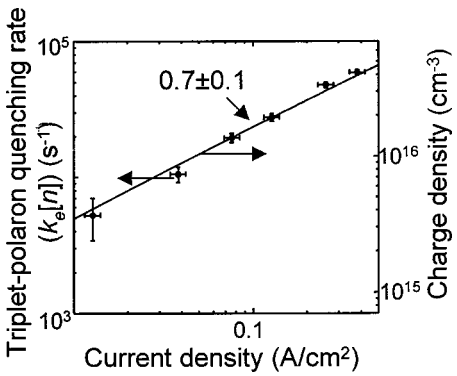

FIG. 8. Variation of charge density n with electron current as determined from the triplet-polaron quenching data of Fig. 7(a), compared to the prediction (solid line) from the J-V characteristics shown in Fig. 7(b).

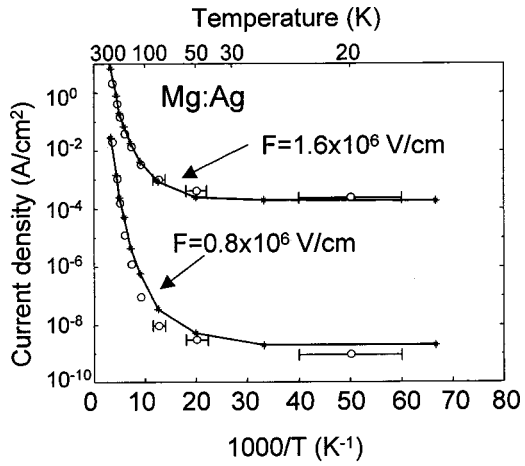

FIG. 9. Dependence of current density on temperature in Alq_3 with a Mg:Ag cathode for two different magnitudes of electric field (○). The activation energy of transport decreases at low temperatures, and transport becomes almost temperature independent for $T<100$ K. The solid line is the temperature dependence of polaron hopping fits to the Mg:Ag/Alq_3 device (see Fig. 10).

function of current density and distance x from the injecting interface, the space-charge density $n(J,x)$ was independently obtained from measurements of polaron-triplet (PT) annihilation, a process occurring when a mobile charge, or polaron, quenches a triplet exciton through inelastic collisions.[7] The density of polarons determines the rate of triplet exciton quenching, which in turn is measured by observing the triplet phosphorescent lifetime.[43] Hence, the precise placement of layers of phosphorescent dopants within a charge transport material allows the space charge to be inferred as a function of position.

The rate of PT interactions is determined using[43]

$$\frac{d[^3M^*]}{dt}=-\frac{[^3M^*]}{\tau}-k_e n(J,x)[^3M^*]-\frac{1}{2}k_{TT}[^3M^*]^2. \tag{17}$$

Here, τ is the natural lifetime of the triplet state, k_e is the rate constant of PT quenching, k_{TT} is the rate of triplet-triplet (TT) annihilation, $[^3M^*]$ is the triplet density, and n is the polaron density. The transient decay, therefore, has linear components and a quadratic component due to bimolecular TT annihilation. Measuring changes in the linear decay rate as a function of current density gives $k_e n(J,x)$, from which the trend in $n(J,x)$ is obtained.

To measure $n(J,x)$, triplets are directly photogenerated on platinum octaethyl porphine (PtOEP), an efficient phosphor[44] whose triplet state has a measured lifetime of $\tau \sim 10\,\mu$s. A pulsed, frequency-doubled Nd-YAG (yttrium aluminum garnet) laser at a wavelength of 532 nm was used to photoexcite PtOEP doped at 8% by mass into a 100-Å-thick layer of Alq_3 (Alq_3 is transparent at this wavelength), and its phosphorescent decay was observed as a function of electron current in Alq_3 [Fig. 7(a)]. The PtOEP-doped Alq_3 layer is incorporated into the device shown in the inset of Fig. 7(a); the J-V characteristics resulting from electron transport in the device are shown in Fig. 7(b) (solid line).

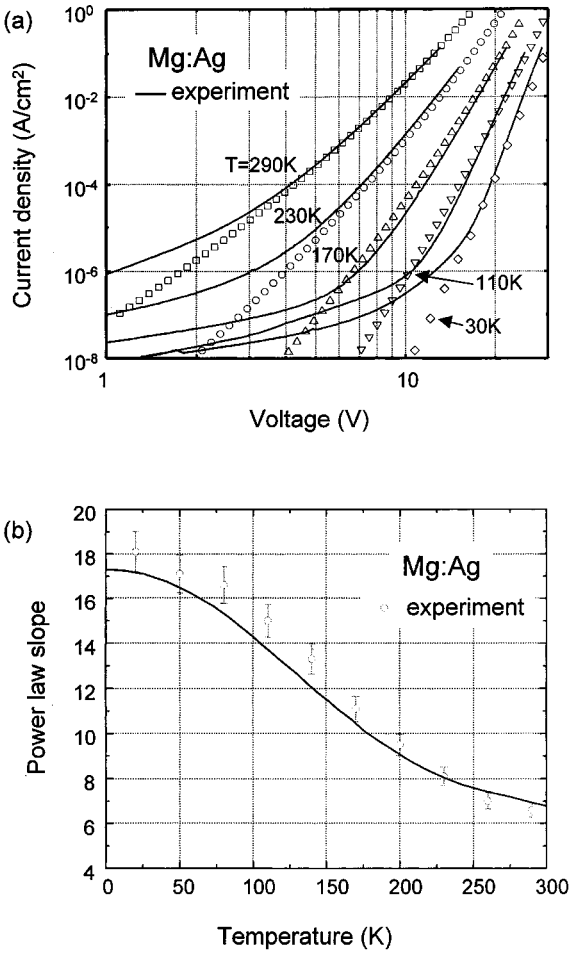

FIG. 10. (a) The temperature dependence of the current-voltage characteristics (solid lines) of Mg:Ag/Alq_3 structures compared to the interface hopping theory described in the text (points). The device structure is Mg:Ag anode/1200 Å Alq_3/1000 Å Mg:Ag/300 Å Ag. The parameters used to calculate injection are given in Table II. (b) The temperature dependence of the power-law slope m, where $J\propto V^m$. The slope levels off at temperatures comparable to the characteristic phonon temperature, $T_P=60$ K. Circles denote the slope of the experimental data between $J=1\times10^{-4}$ A/cm^2 and $J=1\times10^{-2}$ A/cm^2. The solid line is an average of the slopes of the theoretical characteristics over the same range.

It has previously been established that PtOEP is not a strong electron trap in Alq_3,[44] thus observed decreases in the PtOEP triplet lifetime in Fig. 7(a) reflect quenching by Alq_3 polarons. The effect of field dissociation of the triplets which might also lead to a nonlinear optical decay was determined using a device of identical thickness, but with a 300-Å-thick electron blocking injection layer of N,N'-diphenyl-N,N'-bis(3-methylphenyl)-[1,1′-biphenyl]-4,4′-diamine (TPD) positioned adjacent to the cathode. The TPD reduces the current density at a given voltage by over two orders of magnitude; when fields as high as 2×10^6 V/cm are applied, no measurable increase in the PtOEP quenching rate is observed, unambiguously demonstrating that the observed decay is not enhanced by strong external fields.

The polaron quenching rate, $k_e n(J,x)$, is obtained from the data in Fig. 7(a), and assuming that k_e is constant,[45] it is

TABLE II. Parameters for fits to polaron hopping. The width of the bulk distribution (σ_B) was calculated from the dipole moment of Alq_3 using Eq. (2). The transition temperature (T_P) between low- and high-temperature polaron hopping regimes was determined from activation energy plots such as Fig. 9 and measurements of the lattice vibronic spectra of anthracene, naphthalene, and tretracene (Ref. 46). The remaining parameters were obtained by fits to the data. The width of the interface distribution (σ_I) determines the power-law slope of the current-voltage characteristics. Estimations of the effects of semirandom dipole layers at the metal/organic interface show that interface distribution widths of $\sigma_I \sim 0.4$ eV are realistic given a net interfacial dipole of ~1 eV (see Fig. 2). The polaron binding energy E_b and the intermolecular overlap integral (J_0) are verified independently in Monte Carlo simulations in Figs. 14 and 15. For the Alq_3 data, the interfacial site density is normalized to the number of molecules in the first interfacial layer. Thus in the polaron fits, the trap density corresponds to ~20–40 % of sites at the interface. The parameters for PPV are based on data in Campbell *et al.* (Ref. 10). In this case, the width of the bulk distribution (σ_B) is estimated at ~0.1 eV. (b) Parameters for fits to Miller-Abrahams hopping.

(a)

	Fixed parameters			Fit parameters		
Device structure	Polaron transition temperature $T_P=\frac{\hbar\omega_0}{3k_B}$ (K)	Width of bulk distribution σ_B (eV)	Width of interface distribution σ_I (eV)	Polaron binding energy E_b (eV)	Interface site density $N_I d_I$ (cm^{-2})	Intermolecular overlap integral J_0 (meV)
Mg:Ag/Alq_3	60	0.13	0.34	0.16	50×10^{12} (34%)	6
LiF/Al/Alq_3	60	0.13	0.34	0.16	43×10^{12} (30%)	10
Al/Alq_3	60	0.13	0.40	0.10	30×10^{12} (21%)	2
ITO/PPV/Au	60	0.1	0.2	0.17	16×10^{12}	0.1

(b)

Device structure	Width of bulk distribution σ_B (eV)	Width of interface distribution σ_I (eV)	Interface site density $N_I D_I$ (cm^{-2})	Maximum hopping rate A_0 (s^{-1})
Al/Alq_3	0.13	0.40	140×10^{12} (100%)	1×10^{13}

found that $J\propto n^{1.4\pm0.2}$. Assuming a field-independent electron mobility, we expect that an injection-limit should produce ohmic transport characteristics in the bulk where the PtOEP is located, i.e., $J\propto n$. In contrast, bulk-limited transport follows $J\propto n^x$, where $x\geq 2$. When the electric field dependence of mobility is considered, the actual dependence of J on n is greater than expected for a field independent mobility. Consequently, the observation of $J\propto n^{1.4\pm0.2}$ is consistent with injection-limited transport and a weakly field-dependent electron mobility in Alq_3. For example, the relation between J and the interface field $F(0)$ is estimated by fitting the measured J-V characteristics shown in Fig. 7(b), i.e., $J=10^{-10}\times(F(0)d)^{7.6}$ (A/cm^2). Then, using Eqs. (6) and (7), $n(J,x)$ is given by the dashed line in Fig. 8. For these measurements, the electric field, $F=V/d$, ranges from 1.2×10^6 V/cm to 1.9×10^6 V/cm from which we obtain a field-dependent mobility parameter [cf. Eq. (7)], $\alpha=\beta/k_BT_{\rm eff}=(2\pm1)\times10^{-3}\,(\mathrm{V/cm})^{-1/2}$. This compares well to time-of-flight measurements[19] at lower fields ($F<1\times10^6$ V/cm) which give $\alpha=4\times10^{-3}\,(\mathrm{V/cm})^{-1/2}$. Assuming that the zero-field mobility,[19] $\mu_0^*=\mu_0\exp(-E_0/k_BT_{\rm eff})=1\times10^{-6}\,(\mathrm{cm^2/V\,s})$, then $k_e=1\times10^{-12}\,(\mathrm{cm^3/s})$. Overall, the agreement of the steady-state J-V characteristics with the space-charge density expected under an injection limit is excellent, demonstrating that transport in the bulk is ultimately determined by the charge injection properties in the cathode region of the organic film.

VI. TEMPERATURE DEPENDENCE OF THE CURRENT-VOLTAGE CHARACTERISTICS

We now compare measured current-voltage characteristics of the LiF/Al, Mg:Ag, and Al devices with the interfacial hopping theory developed in Sec. III. The temperature de-

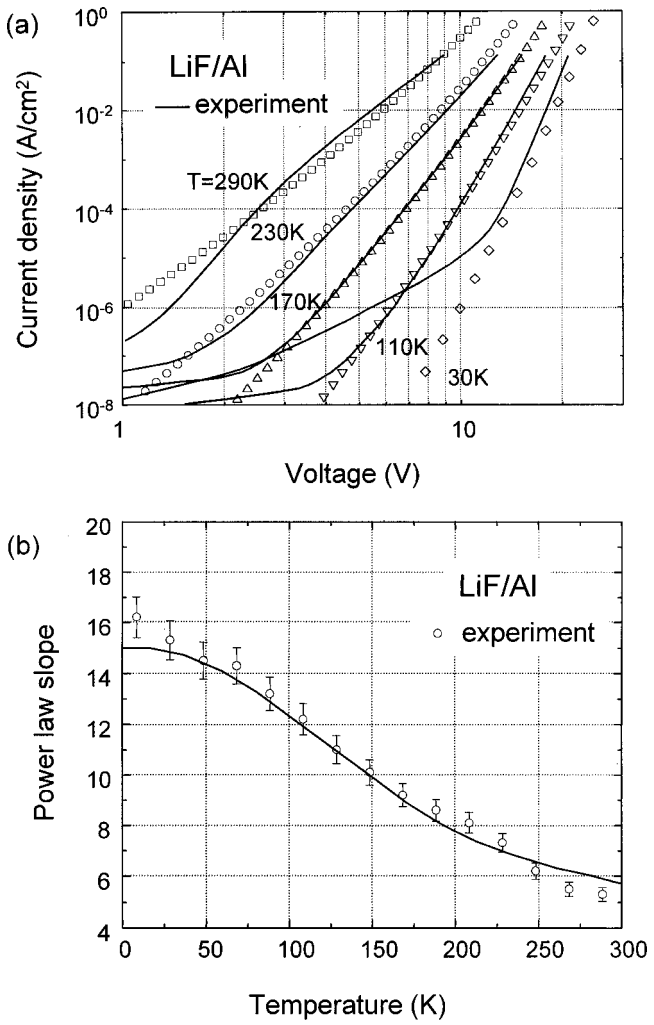

FIG. 11. (a) The temperature dependence of the current-voltage characteristics (solid lines) of Al/LiF/Alq_3 structures compared to the interface hopping theory described in the text (points). The device structure is Mg:Ag anode/1200 Å Alq_3/5 Å LiF/1000 Å Al. The parameters used to calculate injection are given in Table II. (b) The temperature dependence of the power-law slope m, where $J \propto V^m$. The slope levels off at temperatures comparable to the characteristic phonon temperature, $T_P = 60$ K. Circles denote the slope of the experimental data between $J = 1 \times 10^{-4}$ A/cm^2 and $J = 1 \times 10^{-2}$ A/cm^2. The solid line is an average of the slopes of the theoretical characteristics over the same range.

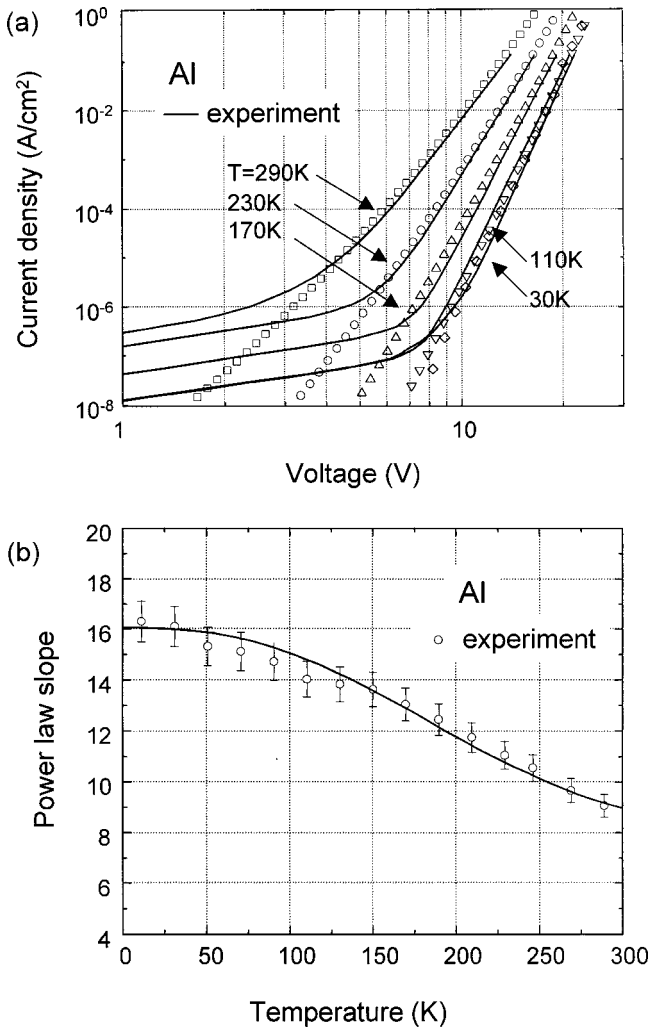

FIG. 12. (a) The temperature dependence of the current-voltage characteristics (solid lines) of Al/Alq_3 structures compared to the interface hopping theory described in the text. The device structure is Mg:Ag anode/1200 Å Alq_3/1000 Å Al. The parameters used to calculate injection are given in Table II. (b) The temperature dependence of the power-law slope m, where $J \propto V^m$. Circles denote the slope of the experimental data between $J = 1 \times 10^{-4}$ A/cm^2 and $J = 1 \times 10^{-2}$ A/cm^2. The solid line is an average of the slopes of the theoretical characteristics over the same range.

pendence of current density in a Mg:Ag/Alq_3 device at a constant voltage is shown in Fig. 9. As described earlier, the departure from a linear, Arrhenius behavior is due to disorder at $T_D \sim 250$ K and the transition from classical to quantum phonon statistics at $T_P \sim 60$ K. To fit this dependence, we note that many of the parameters in our hopping model are already determined, simplifying the procedure. For example, the width of the bulk distribution is taken as $\sigma_B = 0.13$ eV, as calculated in Sec. II for a disordered Alq_3 film. Close to the injecting contact the greater polarizability of the metal surface lowers the mean energy of the interface site distribution.[21] From ultraviolet photoelectron spectroscopy measurements, we take the difference in the mean energies of adjacent molecular layers at the interface as ~0.1 eV.[21] To estimate the optical-phonon energy, $\hbar\omega_0$, we note that the most energetic optical lattice vibrations of naphthalene, anthracene and tetracene are at an energy of approximately $\hbar\omega_0 = 15$ meV.[46] This energy, in turn, corresponds to a phonon-induced transition temperature of $T_P \sim 60$ K, and the approximate temperature independence of the injection current density in Fig. 9 for $T < 100$ K agrees with this estimate of the phonon energy. But we also expect and observe deviations from Arrhenius-like behavior data at higher temperatures, reflecting the effects of disorder. From Eq. (14), we expect that the disorder-induced transition temperature is $T_D \sim 250$ K, consistent with the trend of the data in Fig. 9.

We now proceed to fit the theory of Eqs. (4), (5) and (8) with the temperature-dependent current-voltage characteristics of Mg:Ag devices [solid line, Figs. 9 and 10(b)]. The

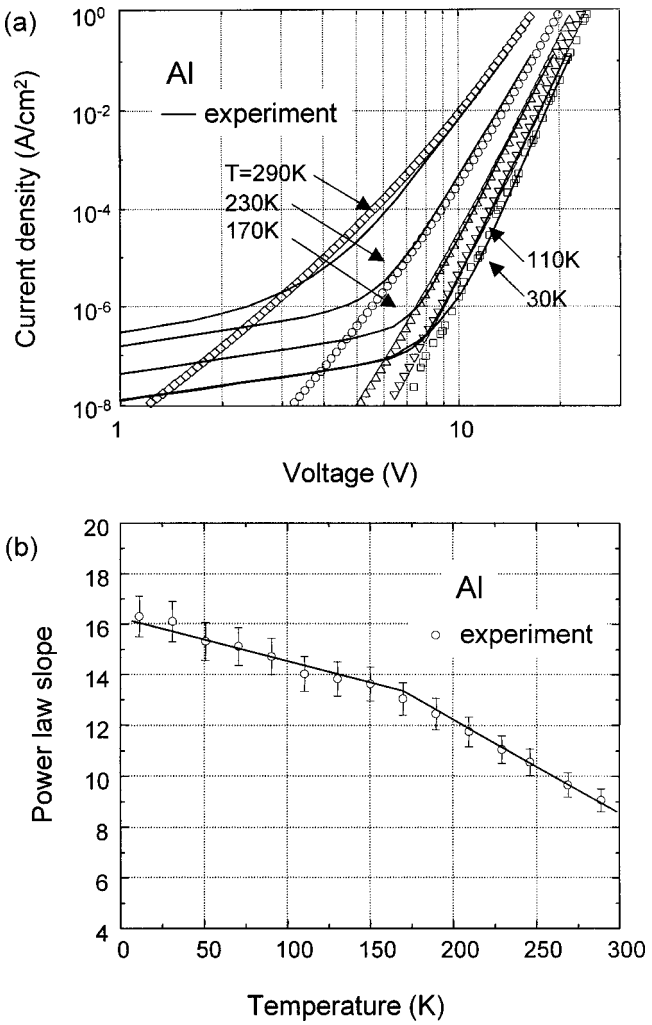

FIG. 13. (a) The temperature dependence of the current-voltage characteristics (solid lines) of Al/Alq_3 devices compared to the interface hopping theory employing Miller-Abrahams rates. The device structure is Mg:Ag anode/1200 Å Alq_3/1000 Å Al. The parameters used to calculate injection are given in Table II. (b) The temperature dependence of the power-law slope m, where $J \propto V^m$. Circles denote the slope of the experimental data between $J=1\times10^{-4}$ A/cm^2 and $J=1\times10^{-2}$ A/cm^2. The solid line is an average of the slopes of the theoretical characteristics over the same range. The fit reproduces the transition in the power law slope data at $T\sim170$ K.

parameters used in the fits are listed in Table II. With minimal variation in the parameters, we are also able to fit the injection characteristics of LiF/Al and Al cathodes in Figs. 11 and 12. At low temperatures (i.e., $k_BT_P<\hbar\omega_0/3$) some quantization is observed in the current-voltage characteristics. This results from our consideration of only a single dominant phonon mode. In part (b) of Figs. 10–12, we show the power-law slope m of the current-voltage characteristics fit to $J\sim V^m$. The power-law slope is a good test of the temperature dependence of transport and injection, particularly at low temperatures, where it has been used previously to highlight the failures of other models.[10]

There are four parameters used in the fits: the polaron binding energy E_b, the polaron bandwidth J_0, the width of

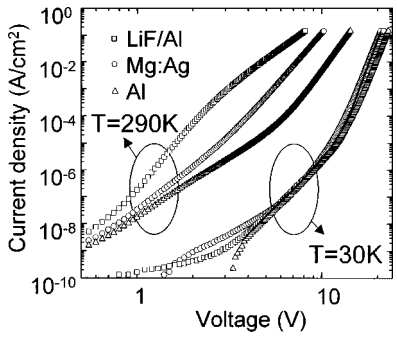

FIG. 14. The current-voltage characteristics of Alq_3 at room temperature and $T=30$ K for a variety of different cathodes. The devices were prepared at the same time for comparative purposes and had the general structure: Mg:Ag anode/1000 Å Alq_3/cathode. From thickness dependence studies of Alq_3 in Fig. 6, transport is found to be injection-limited at $T=30$ K. But at this temperature, the variation in injection characteristics of the different cathode materials disappears, indicating that injection is limited by states in the organic film.

the interfacial site distribution σ_I, and the interfacial site density N_Id_I. Neither the polaron binding energy E_b nor the intermolecular overlap energy J_0, depend significantly on the cathode material. The binding energy was $E_b=(0.14\pm0.04)$ eV, corresponding to a reorganization energy, $\lambda\sim0.3$ eV. Since we expect Marcus inversion of the hopping rate to occur when the free-energy change is equal to the reorganization energy,[39] i.e., when $|\Delta G|=aqF\sim\lambda$, these values of E_b correspond to inversion at an electric-field strength of $F=3\times10^6$ V/cm. Since no evidence for Marcus inversion has been obtained from time-of-flight and transient measurements below this electric field,[19,47] the values of E_b used here are consistent with the upper limit obtained from experiment. At yet higher fields, there is some experimental evidence that the apparent mobility for charge transport decreases in PPV, consistent with $0.1<\lambda<1$ eV.[48] The intermolecular electronic transfer integral J_0 was obtained by fitting the magnitude of the current density. It was found that $J_0=(6\pm4)$ meV. The band associated with electron transport has a half width of $6J_0$;[36] thus as expected, the predicted bandwidth of these materials ($\sim$40 meV) is significantly less than the polaron binding energy. These parameter values are tested further in Sec. VII using a Monte Carlo simulation to predict the field-dependent mobility of bulk transport in Alq_3.

The width of the interfacial site distribution σ_I and the interfacial surface density of states N_Id_I are also consistent with our interfacial dipole model. From Fig. 2 we infer that strong dipole fields at the metal/organic interface can result in an interfacial site distribution of width $\sigma_I=0.35$ eV, similar to that observed in fits of data from Mg:Ag, LiF/Al, and Al cathodes. The density of interface states N_Id_I was obtained by fitting the voltage data. As shown in Table II, we find that N_I is on the order of the molecular density at the interface.

As confirmation of the importance of disorder, we note that for the Al cathode it is also possible to fit the data with the simplified Miller-Abrahams hopping model. This model

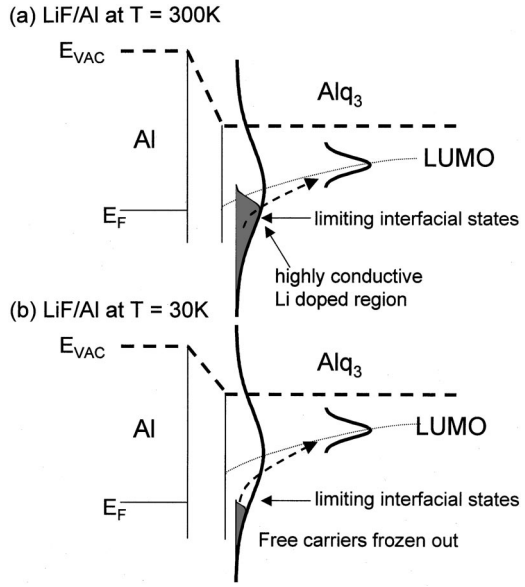

FIG. 15. The temperature dependence of a LiF/Al cathode on Alq_3 can be explained by the low-temperature freeze out of free carriers due to Li doping. (a) At room temperature, the surface of the Alq_3 is highly conductive due to the Li doping, thus the effective injection interface moves into the bulk of the organic, away from the interfacial dipole layer. The dotted line indicates the mean energy of the charge distribution as a function of position in the thin film. (b) At low temperature, the free charge is frozen out, and injection occurs directly from the distribution of interfacial sites. Consequently, at low temperatures, LiF/Al cathodes behave similarly to Al cathodes.

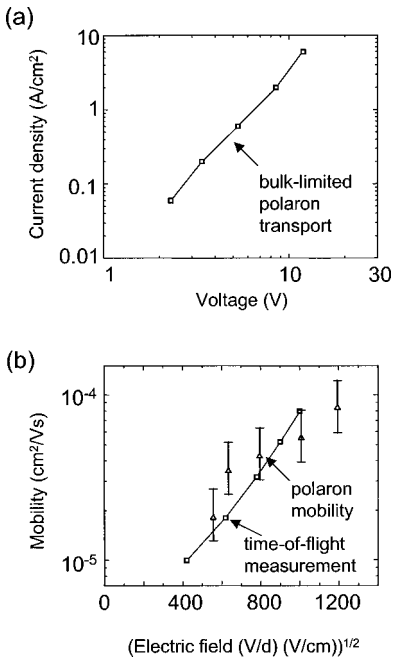

FIG. 16. (a) The J-V characteristic obtained from Monte Carlo simulations of bulk transport in Alq_3. Room-temperature characteristics for the polaron simulation with $\lambda = 0.3$ eV, $\sigma = 0.13$ eV, and $J_0 = 6$ meV. (b) The macroscopic mobility is extracted from the polaron simulation data (□) and time-of-flight data from Chen and Liu (Ref. 19) (△). Note that we have plotted the mobility versus the macroscopic parameter V/d rather than the electric field F. The error in the simulated mobility is estimated from the variation in the maximum hopping rate in polaron fits to Mg:Ag/Alq_3, Al/LiF/Alq_3, and Al/Alq_3 (see Table II).

does not contain the parameters E_b, J_0, or $\hbar\omega_0$, and its temperature dependence is solely determined by the effects of disorder in the molecular film. We fit the Al data using $\sigma_I = 0.4$ eV and a maximum hopping rate of $A_0 = 1 \times 10^{13}\,\mathrm{s}^{-1}$. The power-law slopes of the current-voltage characteristics for injection from the Al cathode are also shown in Fig. 13. Considering that there are *no* temperature-dependent parameters, it is remarkable that the theory reproduces an apparent kink in the power-law data at $T \sim 170$ K.

The only apparent discrepancy in the application of the interface-limited theory is the variation in the Alq_3 polaron parameters E_b and J_0 that is observed in fits to the different cathodes. This reflects the variation in cathode injection efficiencies at room temperature. However, it is interesting that at very low temperatures ($T \lesssim 30$K), all the cathodes possess nearly identical current-voltage characteristics (see Fig. 14). This unambiguously breaks the link between the cathode work function and its injection efficiency, demonstrating that the initial hop from the metal Fermi level into the organic is not the most energetically costly even in current injection. Since the injection characteristics are determined by the interface distribution, the similarity at $T \sim 30$ K suggests that the organic interfacial site distributions are similar for all contacts. The more pronounced temperature dependence of injection from LiF/Al cathodes is therefore explained by the freezing out of free charge introduced by Li doping.[49] Similarly, Mg may also dope the interfacial layers of Alq_3. In both cases, the doping is concentrated in the region most affected by interfacial dipolar disorder, making that region highly conductive at room temperature. Thus LiF/Al cathodes improve injection by raising the Fermi energy and shifting the effective injection interface deeper into the organic film where the distribution of organic states is narrower and the

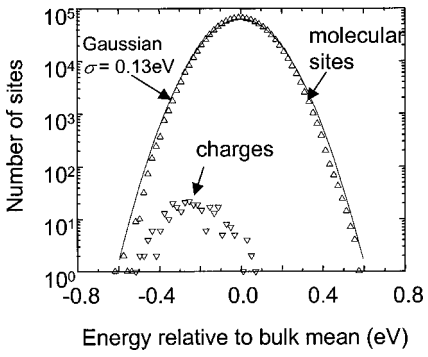

FIG. 17. The electron-energy distribution calculated using a Monte Carlo simulation of polaron hopping rates. The charges do not fully relax during their transit across the 1000-Å-thick film. The data are shown 10 ns after the application of a step function corrent density of $J = 300$ A/cm^2. For comparison we also show the total molecular density of states used in simulating bulk transport in Alq_3. The density of states is approximately Gaussian with a width of $\sigma = 0.13$ eV, and the reorganization energy is $\lambda = 0.5$ eV.

hopping barrier to injection is reduced.

The proposed mechanism for injection from the LiF/Al cathode is shown in Fig. 15. However, the temperature dependence of extrinsic material properties, such as doping, is not considered in the theory of Sec. III. Its presence causes artifacts in the fit, which might result in apparent variations in the Alq_3 polaron parameters. Thus, fits to the Al data (see Figs. 12 and 13) may be the most accurate source of Alq_3 polaron parameters because the Al cathode introduces less free charge into the interfacial organic layer. Correspondingly, we are able to fit both the temperature and thickness dependence of transport in Al/Alq_3 devices using the simplified Miller-Abrahams hopping model and only two free parameters.

VII. MONTE CARLO MODELING OF BULK TRANSPORT

To verify the self-consistency of the theory, we use the Alq_3 polaron parameters E_b and J_0 to calculate the bulk mobility, and then compare those results to the measured value. A Monte Carlo model was used to analyze an ordered array of Alq_3 sites with dimensions $101\times101\times100$ and an intersite spacing of 10 Å. Two simplifications are employed: only nearest-neighbor hops are considered,[38] and we ignore off-diagonal disorder, i.e., positional disorder in the organic film. Measurements[19,50] of the mobility of Alq_3 show that μ increases with electric field for $F<10^6$ V/cm, as is expected in the absence of strong positional disorder effects.

Monte Carlo models become increasingly computationally demanding as $\sigma/k_BT\gg1$ because of the difficulty in simulating the extreme tail of the density of states. Hence the calculations were restricted to room temperature where downward jumps into the tail of the distribution are less important. We use the high-temperature rate [Eq. (11)] to model charge transport. Energetic disorder is introduced by assigning each site a randomly directed dipole moment of strength $p=5.3$ D. The site energies are then calculated according to the correlated disorder model,[29] yielding an approximately Gaussian distribution with $\sigma_B=0.13$ eV. To set the current density we introduce charges at a given rate into random sites in the first layer. The time interval is 1 ps.

In Fig. 16(a) we plot the simulated current-voltage characteristics at $T=300$ K. Comparison with Figs. 10–13 demonstrates that under these conditions, the bulk is much less resistive than the injection interface, supporting our finding of injection-limited behavior in these devices. In Fig. 16(b) we plot the macroscopic electron mobility (i.e., $\mu=8Jd^3/9\varepsilon V^2$) extracted from the transport data in Fig. 16(a). It is clearly temperature and field dependent, in agreement with previous studies of polaron hopping in disordered organic films.[38,40] For comparison we plot the time-of-flight mobility measurements of Chen and Liu,[19] and observe that the model shows reasonable agreement with experiment. At $V/d=1\times10^6$ V/cm, time-of-flight measurements give $\mu=8\times10^{-5}$ cm^2/V s,[19] which compares to the simulated small polaron mobility of $\mu=(6\pm3)\times10^{-5}$ cm^2/V s.

Finally, we note that the charges within the simulated Alq_3 film do not fully relax during their transit. Figure 17 compares the total molecular density of states to the charge density distribution. The data are taken 10 ns (10^4 time intervals) after a current density of $J=300$ A/cm^2 is injected into an 1000-Å-thick Alq_3 film. As expected, the total density of states is approximately Gaussian, with a width of $\sigma_B=0.13$ eV. The energy distribution of charges relative to the bulk mean is also Gaussian, and the lowest-energy sites are observed to remain unfilled well after the current density has stabilized. This result suggests that we may generalize the model to consider injection across an interface that possesses an equilibrium population of carriers on one side but not on the other. In the case of Alq_3 in contact with a low work-function cathode, the small energy barrier between the cathode and the interface states does not prevent an equilibrium distribution in the organic interfacial states. On the other side of the interface, several reasons may account for nonequilibrium transport: firstly, a high density of interface charge establishes a strong internal field that lowers the local Fermi energy, thereby discouraging electron trapping; and secondly, transport in the bulk is expected to be dominated by percolation paths of near-resonantly-coupled molecules, narrowing the effective density of states. In this work we have only considered metal/Alq_3 devices where the injection interface is within the first few layers of the organic film, but it is possible that other material systems will vary. For example, in the absence of interfacial dipoles, the equilibrium/nonequilibrium interface can occur directly at the organic/metal boundary, giving injection characteristics that are strongly dependent on the work function of the metal. Or, if the organic is doped and there is a high free-carrier concentration in the vicinity of the cathode, the interface boundary may occur deeper within the organic film. As the LiF/Al cathode demonstrates, this provides a technique for improving the performance of injection contacts; free charges from the dopant can assist charge transport in the region where the interfacial dipoles have significantly broadened the energetic distribution of molecular states.

VIII. DISCUSSION

We have concentrated thus far on the small molecule, electron transport material, Alq_3. Many other studies[8,10,31] have examined charge transport in the conjugated polymer, PPV. Although it is not our intention to study this material in detail, we note that when transport in PPV is injection limited, the same theory may also be used to explain the temperature dependence of the current-voltage characteristics. In Fig. 18 we reproduce the power-law slope data for injection-limited ITO/dialkoxy-PPV/Au devices of Campbell *et al.*[10] Although these devices exhibit large leakage currents that obscure the power law at room temperature, at low temperatures the current-voltage characteristics are similar to those observed for injection into Alq_3. In the polymer devices, however, the injection interface is believed to be the ITO/dialkoxy-PPV contact.[10] The polymer devices therefore differ from the Alq_3 devices in this work by being hole-injection devices and by having their injection interface formed by organic rather than by metal deposition. Never-

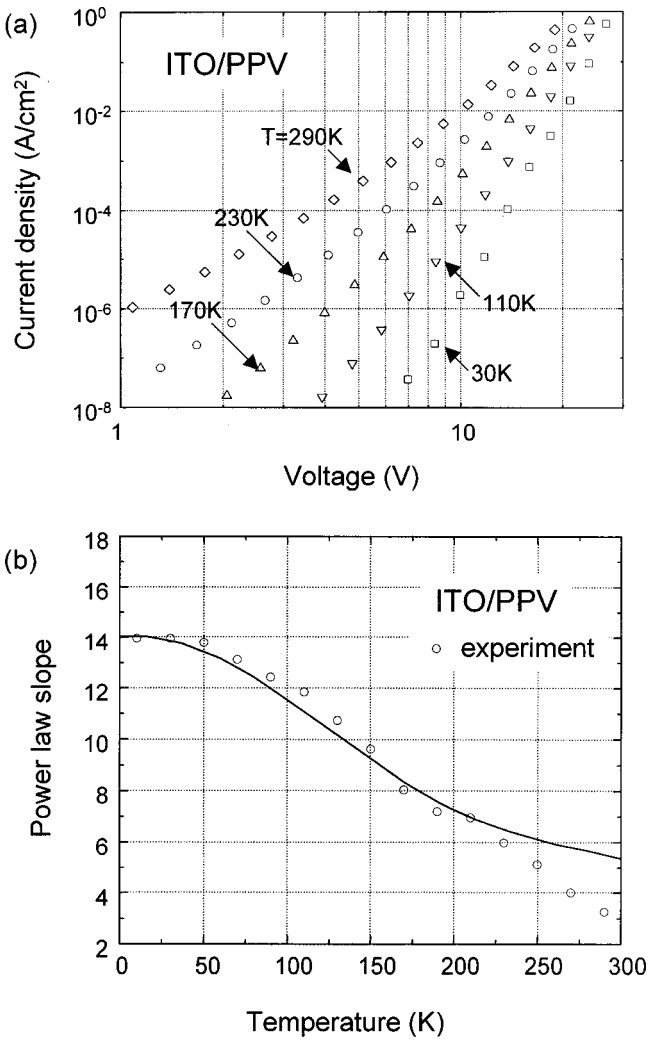

FIG. 18. (a) Calculated temperature dependence of the current-voltage characteristics of polymer, hole-only devices with the structure ITO/900Å dialkoxy-PPV/Au using the theory discussed in the text. The parameters used to calculate injection are given in Table II. The current-voltage characteristics should be compared with Fig. 2 in Campbell *et al.* (Ref. 10). (b) The temperature dependence of the power-law slope m, where $J \propto V^m$. The data are compared with Campbell *et al.* (Ref. 10). Circles denote the slope of the experimental data. The solid line is an average of the slopes of the theoretical characteristics between $J=1\times10^{-2}$ A/cm^2 and $J=1\times10^{-1}$ A/cm^2. Large leakage currents lead to uncertainties in the room-temperature data, possibly altering the apparent power-law slope.

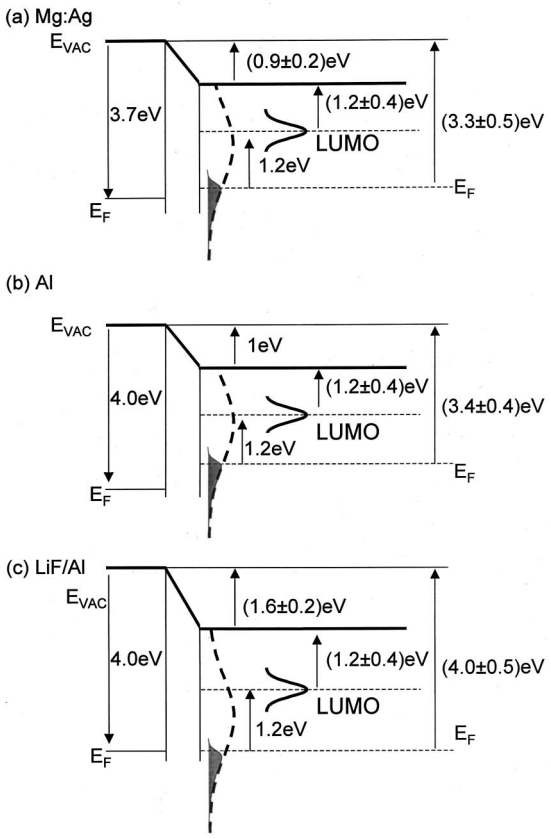

FIG. 19. The energy-level diagrams for (a) Mg:Ag, (b) Al, and (c) LiF/Al cathodes on Alq_3. UPS data from Table I are used to calculate the relative positions of the metal work function, vacuum level in the metal and organic, and organic LUMO. We compare the UPS data to the Fermi level in the organic interfacial states, as obtained from polaron fits at a low current density ($J\sim10^{-8}$ A/cm^2). The energy barrier between the metal and the organic interfacial states for the LiF/Al cathode at $J\sim10^{-8}$ A/cm^2 is (0.0 ± 0.5) eV. The energy barriers for the Mg:Ag and Al cathodes are (0.4 ± 0.5) eV and (0.6 ± 0.4) eV, respectively, at $J\sim10^{-8}$ A/cm^2, suggesting that injection is not completely independent of the contact for higher work-function materials such as Al.

theless, the temperature dependence of the power-law slope can also be fit by the parameters given in Table II. As compared to the results for electron injection into Alq_3, we observe that dialkoxy-PPV has a lower polaron binding energy E_b and a lower bandwidth $6J_0$. Since the hopping rate (and hence the mobility) is proportional to J_0^2, the lower intermolecular overlap energy, $J_0=0.1$ meV, corresponds to a maximum hopping rate of $\sim3\times10^8$ s^{-1}, as compared to that of Alq_3 polarons of $\sim2\times10^{11}$ s^{-1}. A comparison of the current-voltage characteristics of this dialkoxy-PPV with the characteristics of other[8,31] (bulk-limited) PPV samples which possess a mobility similar to that of Alq_3 suggests that the mobility of this dialkoxy-PPV should indeed be much lower. In any case, the fit to these data at $300<T<10$ K demonstrates the generality of the interfacial injection model.

Figure 19 shows the proposed energy-level diagrams for the Mg:Ag, Al, and LiF/Al cathodes on Alq_3. We compare UPS data from Table I with the Fermi level in the organic interfacial states, as obtained from polaron fits at a low current density ($J\sim10^{-8}$ A/cm^2). In accordance with expectations, we find that the interfacial states and the metal are approximately in equilibrium at low current densities, and that the largest barrier is between the interface states and the bulk organic states. This is especially true for the LiF/Al cathode which has a barrier between the Al contact and the Alq_3 at $J\sim10^{-8}$ A/cm^2 of (0.0 ± 0.5) eV. The Mg:Ag and Al contacts have barriers of (0.4 ± 0.5) eV and (0.6 ± 0.4) eV, respectively, at $J\sim10^{-8}$ A/cm^2, confirming that the organic interfacial/bulk energy barrier remains dominant. The error

in the determination of the barrier between Al and Alq_3 does not include measurement errors in the interface dipole field, and therefore it should be considered an underestimate. Note also that the broad distribution of interfacial Alq_3 molecules shown in Fig. 19 should be distinguished from the lower-lying ''gap states'' observed in UPS, which probably originate from chemical damage inflicted on the organic during deposition of such low work-function metals as Li, Mg, and Al.[26,49,51,52]

Of the various models competing to explain the transport characteristics of amorphous semiconductor materials, two approaches have proved attractive: starting from the observed shape and temperature dependence of transport, trapped charge models[4,10,11] have been used to accurately describe characteristics for $T>100\,\mathrm{K}$; and starting from a fundamental understanding of charge transport in amorphous materials, ''disorder'' models have been used to explain the field and temperature dependence of charge mobility.[53] In some respects, the interfacial model is a synthesis of these approaches. The broad density of states at the interface and the narrower bulk distribution is qualitatively similar to trapped charge limited models, and it generates the correct power-law dependencies. But the interfacial model requires energetic disorder in the bulk and dipole-induced disorder at the interface to explain these distributions. In doing so, it seeks to provide a macroscopic model of charge hopping in amorphous semiconductors.

IX. CONCLUSION

We have demonstrated that for three commonly used cathodes (Mg:Ag, LiF/Al, and Al), electron transport in the archetype amorphous organic semiconductor Alq_3 is dominated by injection processes which are in turn influenced by states at the metal/Alq_3 interface. It is observed that a broad, dipole-induced, Gaussian distribution of sites at the interface creates sufficient energetic disorder to dominate the transport characteristics, yielding the power laws commonly observed in the current-voltage characteristics of many amorphous organic semiconductor thin-films. Indeed, using a simplified model of charge hopping that ignores the phonon distribution, we are able to fit the temperature and thickness dependence of transport in Al/Aq_3 devices using the simplified Miller-Abrahams hopping model and only two free parameters. Using a more sophisticated model of polaron hopping we have found that the parameters used to describe Alq_3 polarons in fits of the injection characteristics are consistent with Monte Carlo simulations of bulk-limited transport in Alq_3 at room temperature. In addition, we found that the model could be extended to injection-limited metal-polymer interfaces such as ITO/dialkoxy-PPV.

But to gain a more fundamental understanding of charge injection at metal/organic interfaces, we must derive the energetic distribution of interface states. We must also understand the chemistry at the interface: in particular, the physical origins of interface dipoles that lead to a lowering of the interface energy barrier and determine the width of the interfacial state distribution. Once both the origin and distribution of interface states and the intermolecular overlap integrals are quantified, methods for the molecular scale manipulation of injection interfaces may become possible.

ACKNOWLEDGMENTS

The authors thank Peter Peumans, Zoltan Soos, and Antoine Kahn for insightful discussions. This work was supported by Universal Display Corporation, the Defense Advanced Research Projects Agency, the Air Force Office of Scientific Research, and the National Science Foundation MRSEC program.

[1] U. Wolf, V. I. Arkhipov, and H. Baessler, Phys. Rev. B **59**, 7507 (1999).
[2] V. I. Arkhipov, U. Wolf, and H. Baessler, Phys. Rev. B **59**, 7514 (1999).
[3] S. Barth, U. Wolf, H. Baessler, P. Mueller, H. Riel, H. Vestweber, P. F. Seidler, and W. Riess, Phys. Rev. B **60**, 8791 (1999).
[4] P. E. Burrows, Z. Shen, V. Bulovic, D. M. McCarty, S. R. Forrest, J. A. Cronin, and M. E. Thompson, J. Appl. Phys. **79**, 7991 (1996).
[5] M. Stoessel, J. Staudigel, F. Steuber, J. Blaessing, and J. Simmerer, Appl. Phys. Lett. **76**, 115 (2000).
[6] S. Barth, H. Baessler, D. Hertel, V. I. Nikitenko, and U. Wolf, Pure Appl. Chem. **71**, 2067 (1999).
[7] M. Pope and C. Swenberg, *Electronic Processes in Organic Crystals* (Oxford University Press, Oxford, 1982).
[8] P. W. M. Blom, M. J. M. d. Jong, and M. G. v. Munster, Phys. Rev. B **55**, 656 (1997).
[9] M. A. Lampert and P. Mark, *Current Injection in Solids* (Academic Press, New York, 1970).
[10] A. J. Campbell, M. S. Weaver, D. G. Lidzey, and D. D. C. Bradley, J. Appl. Phys. **84**, 6737 (1998).
[11] A. J. Campbell, D. D. C. Bradley, and D. G. Lidzey, J. Appl. Phys. **82**, 6326 (1997).
[12] L. S. Hung, C. W. Tang, and M. G. Mason, Appl. Phys. Lett. **70**, 152 (1997).
[13] I. D. Parker, J. Appl. Phys. **75**, 1656 (1994).
[14] S. M. Sze, *Physics of Semiconductor Devices* (Wiley, New York, 1981).
[15] A. J. Campbell, D. D. C. Bradley, J. Laubender, and M. Sokolowski, J. Appl. Phys. **86**, 5004 (1999).
[16] C. W. Tang and S. A. VanSlyke, Appl. Phys. Lett. **11**, 913 (1987).
[17] G. Parthasarathy, C. Adachi, P. E. Burrows, and S. R. Forrest, Appl. Phys. Lett. **76**, 2128 (2000).
[18] H. Ishii, K. Sugiyama, E. Ito, and K. Seki, Adv. Mater. **11**, 605 (1999).
[19] B. Chen and S. Liu, Synth. Met. **91**, 169 (1997).
[20] I. G. Hill, A. Rajagopal, A. Kahn, and Y. Hu, Appl. Phys. Lett. **73**, 662 (1998).
[21] I. G. Hill, A. J. Makinen, and Z. H. Kafafi, Appl. Phys. Lett. **77**, 1825 (2000).

[22] R. Schlaf (private communication).
[23] G. Parthasarathy, P. E. Burrows, V. Khalfin, V. G. Kozlov, and S. R. Forrest, Appl. Phys. Lett. **72**, 2138 (1998).
[24] V. Bulovic, P. Tian, M. R. Gokhale, and S. R. Forrest, Appl. Phys. Lett. **70**, 2954 (1997).
[25] M. Probst and R. Haight, Appl. Phys. Lett. **70**, 1420 (1997).
[26] A. Rajagopal and A. Kahn, J. Appl. Phys. **84**, 355 (1998).
[27] J. C. Scott and G. C. Malliaras, Chem. Phys. Lett. **299**, 115 (1999).
[28] A. Dieckmann, H. Baessler, and P. M. Borsenberger, J. Chem. Phys. **99**, 8136 (1993).
[29] R. H. Young, Philos. Mag. B **72**, 435 (1995).
[30] R. L. Martin, J. D. Kress, I. H. Campbell, and D. L. Smith, Phys. Rev. B **61**, 15 804 (2000).
[31] W. D. Gill, J. Appl. Phys. **55**, 5033 (1972).
[32] P. W. M. Blom, M. J. M. de Jong, and J. J. M. Vleggaar, Appl. Phys. Lett. **68**, 3308 (1996).
[33] R. A. Marcus, J. Chem. Phys. **24**, 966 (1955).
[34] T. Holstein, Ann. Phys. (N.Y.) **8**, 325 (1959).
[35] T. Holstein, Ann. Phys. (N.Y.) **8**, 343 (1959).
[36] D. Emin, Adv. Phys. **8**, 305 (1975).
[37] D. Emin, Phys. Rev. B **4**, 3639 (1971).
[38] Y. N. Gartstein and E. M. Conwell, Chem. Phys. Lett. **217**, 41 (1994).
[39] G. L. Closs and J. R. Miller, Science **240**, 440 (1988).
[40] Z. G. Soos, S. Bao, J. M. Sin, and G. W. Hayden, Chem. Phys. Lett. **319**, 631 (2000).
[41] S. Barth, D. Hertel, Y.-H. Tak, H. Baessler, and H. H. Hoerhold, Chem. Phys. Lett. **274**, 165 (1997).
[42] S. R. Forrest, Chem. Rev. **97**, 1793 (1997).
[43] M. A. Baldo, C. Adachi, and S. R. Forrest, Phys. Rev. B **62**, 10 967 (2000).
[44] M. A. Baldo and S. R. Forrest, Phys. Rev. B **62**, 10 958 (2000).
[45] The triplet-polaron model neglects polaron collisions involving more than one other species. This is justified for low densities of polarons and triplets, as used in our studies.
[46] E. A. Silinsh and V. Capek, *Organic Molecular Crystals: Interaction, Localization, and Transport Phenomena* (AIP, New York, 1994).
[47] C. Hosokawa, H. Tokailin, H. Higashi, and T. Kusumoto, Appl. Phys. Lett. **60**, 1220 (1992).
[48] N. Tessler, N. T. Harrison, and R. H. Friend, Adv. Mater. **10**, 64 (1998).
[49] Q. T. Le, L. Yan, Y. Gao, M. G. Mason, D. J. Giesen, and C. W. Tang, J. Appl. Phys. **87**, 375 (2000).
[50] S. Naka, H. Okada, H. Onnagawa, Y. Yamaguchi, and T. Tsutsui, Synth. Met. **111–112**, 331 (2000).
[51] C. Shen, I. G. Hill, A. Khan, and J. Schwartz, J. Am. Chem. Soc. **122**, 5391 (2000).
[52] S. T. Lee, X. Y. Hou, M. G. Mason, and C. W. Tang, Appl. Phys. Lett. **72**, 1593 (1998).
[53] P. M. Borsenberger, E. H. Magin, M. van der Auweraer, and F. C. de Schryver, Phys. Status Solidi **140**, 10 (1993).
[54] I. G. Hill, A. Kahn, Z. G. Soos, and R. A. Pascal, Chem. Phys. Lett. **327**, 181 (2000).
[55] R. Schlaf, B. A. Parkinson, P. A. Lee, K. W. Nebesny, G. Jabbour, B. Kippelen, N. Peyghambarian, and N. R. Armstrong, J. Appl. Phys. **84**, 6729 (1998).
[56] A. Kahn (private communication).
[57] C. Shen, I. G. Hill, and A. Kahn, Adv. Mater. **11**, 1523 (1999).